Eur. Phys. J. B **32**, 237–242 (2003)
DOI: 10.1140/epjb/e2003-00093-7

THE EUROPEAN PHYSICAL JOURNAL B

Study of the sound-vortex interaction: direct numerical simulations and experimental results

R. Berthet[1,a], S. Fauve[1], and R. Labbé[2]

[1] LPS[b], École Normale Supérieure, 24 Rue Lhomond, 75231 Paris Cedex 05, France
[2] Laboratorio de Turbulencia, Departamento de Física, Universidad de Santiago de Chile, Casilla 307, Correo 2, Santiago, Chile

Received 9 October 2002 / Received in final form 20 January 2003
Published online 1st April 2003 –

Abstract. We present a study of sound propagation through a single vortex by direct numerical simulations (DNS) compared to experimental measurements. We analyse the amplitude and the phase shift of the sound wave when it interacts with the vortical flow and we display the focusing effects produced by the vortex. We show that the turbulent fluctuations have a little effect on the sound phase shift whereas they induce a strong defocusing effect on the sound amplitude.

PACS. 43.28.+h Aeroacoustics and atmospheric sound – 47.32.-y Rotational flow and vorticity

1 Introduction

The scattering of sound by turbulent and vortical flows has been extensively studied experimentally and analytically. Despite this large amount of data, the respective contributions of large structures of the mean flow in the scattering processes is not clearly established. In experimental situations [1–7], this comes from two major difficulties: first, it is not possible to separate the scattered signal from the full sound wave and second, it is hard to change independently the amplitude of the large scale vortical flow and the turbulent fluctuations.

Analytical studies are usually limited to study the interaction between a sound wave (wavelength λ) and an isolated stationary vortex (typical size L) with a small Mach number $\mathcal{M} \ll 1$. In the geometrical limit $\lambda \ll L$, one can use standard ray-tracing techniques to qualitatively analyze the spatial acoustic energy repartition [8]. In the large wavelength limit $\lambda \gg L$, the scattered wave can be computed with partial-wave method [9–11]. Asymptotic expansions can also be used in this limit [12]. Born approximations can be applied to the sound scattering problem in a third limit. In the first Born approximation (single scattering limit, $\mathcal{M}L/\lambda \ll 1$), the full structure of the scattered wave can be obtained in the far-field limit [13,14] but the approximation usually breaks down in the forward direction for non-zero circulation vortices [15,16]. More recently, the case of many vortices has been considered and the sound propagation has been studied in the second Born approximation [17,18].

In this paper, we analyze the whole structure of the scattered wave (amplitude and phase) using direct numerical simulations (DNS). We compare them with experimental results obtained in a parameter range for which the various approximations quoted above are not valid. The experimental and numerical approaches complement each other to give a good understanding of the scattering process. To our knowledge, this is the first time this kind of comparison between experimental and numerical results is performed for sound scattering by vorticity.

The paper is organised as follow: after a short presentation of the experimental setup and of the numerical methods, we analyse the phase and the amplitude of the sound wave. Then, we compare the numerical results with experimental measurements and we show the effect of turbulent fluctuations on the scattering process.

2 Experimental setup

The experimental setup has been already described in [19]. The flow is driven by two coaxial centrifugal fans – with diameter 0.2 m – facing each other, 0.3 m apart and rotating at 27 Hz in the same direction. A strongly turbulent vortex (Reynolds number greater than 10^5) is generated and performs a slow precession motion around the common rotation axis of the disks. The trajectory of its core is nearly circular with radius approximately 0.025 m. A square capacitive transducer (0.16 m × 0.16 m) is used

[a] e-mail: rberthet@lps.ens.fr
[b] UMR CNRS 8550

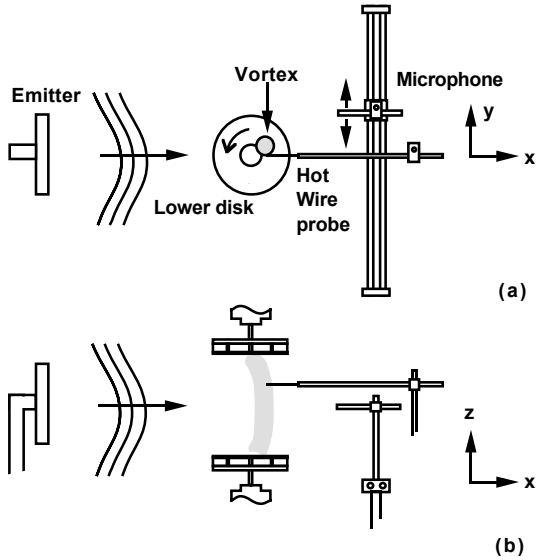

Fig. 1. Experimental set-up. (a) Upper view, with the vortex represented as a shadowed circle. (b) Side view.

to send an ultrasonic wave onto the vortex. The sound frequency is $\nu_0 = 34$ kHz, so that the corresponding wavelength, $\lambda \sim 0.01$ m, is of the same order as the diameter $d \sim 0.02{-}0.04$ m of the vortex core. The emitter is 1 m far from the rotation axis. A schematic drawing of the experimental setup is shown in Figure 1.

The effect of the vortex on the sound wave is obtained by comparing the wave fronts propagated in still air with the ones produced in the presence of the vortex. The sound detector is a miniature microphone located 0.3 m behind the vortex; its distance to the propagation line (y coordinate in Fig. 1a) can be freely adjusted. The measured signal is first processed by a lock-in amplifier and then subjected to an adaptive coherent average to remove the fluctuations induced by the vortex precession and the turbulence background [20]. This is done with the help of a signal provided by a hot wire anemometer which allows, after some processing, to find the instantaneous position of the vortex. This procedure gives both, the amplitude and the phase of the sound wave as functions of the distance to the propagation line and time.

3 Numerical modelisation

Numerical simulations offer a powerful and accurate tool for the study of the sound scattering process: they allow the full and direct observation of the scattered wave, the analysis of the sound wave-mean flow interactions and they provide complementary results to experimental data [21]. As pointed out by Colonius *et al.* [22], the direct numerical simulation of such a problem is very difficult because several spatial scales (typical size of the mean flow and wavelength of the sound wave) must be considered together. Another major difficulty arises from the fact that the amplitude of the different physical phenomena range over several orders of magnitude. The scattered wave amplitude is usually one or two orders of magnitude smaller than the incident sound wave amplitude which is itself four orders of magnitude smaller than the amplitude of the mean flow. Thus, when designing a numerical code for sound scattering computations, the interior discretization scheme has to be chosen with care to ensure high quality dispersion and diffusion properties. Moreover, a proper boundary algorithm is needed to avoid as much as possible the parasitic reflection of outgoing sound waves on the domain boundaries [23].

3.1 Computationnal algorithm

The algorithm solves the conservation equations governing the time evolution of a compressible, isothermal and non-viscous flow in a two-dimensional case:

$$\frac{\partial U}{\partial t} + \frac{\partial F}{\partial x} + \frac{\partial G}{\partial y} = 0 \tag{1}$$

with

$$U = \begin{pmatrix} \rho \\ \rho u \\ \rho v \\ E \end{pmatrix} \; F = \begin{pmatrix} \rho u \\ \rho uu + p \\ \rho vu \\ (E+p)u \end{pmatrix} \; G = \begin{pmatrix} \rho v \\ \rho uv \\ \rho vv + p \\ (E+p)v \end{pmatrix} \tag{2}$$

ρ, u, v, E and p denote respectively the density, the fluid velocity components in the x and y Cartesian directions, the total energy (kinetic energy and internal energy) and the pressure. Assuming a perfect gas and neglecting thermal effects, the pressure can be written as follows:

$$p = (\gamma - 1)\left(E - \frac{1}{2}\rho(u^2 + v^2)\right). \tag{3}$$

The interior scheme is based on an enhanced version of the Mac Cormack's scheme. Using a predictor-corrector technique, this scheme is second order accurate in time and fourth order accurate in space [24]. The boundary algorithm uses a linear decomposition of the physical fields $U(t)$ with respect to the initial state of the simulation and an approach using a characteristics method. It allows a great numerical stability of the mean flow and low boundary reflections during the sound-flow computation [23].

3.2 Numerical setup

An Oseen vortex seems to be the closest mean flow model to analyze our sound scattering problem. Its vorticity field $\mathbf{\Omega}(\mathbf{r})$ can be expressed in cylindrical coordinates [25]

$$\mathbf{\Omega}(\mathbf{r}) = \Omega_0 \exp\left[-\alpha \frac{r^2}{L^2}\right] \hat{z} \tag{4}$$

which corresponds to the velocity field

$$\mathbf{v}(\mathbf{r}) = \frac{\Gamma}{2\pi r}\left(1 - \exp\left[-\alpha \frac{r^2}{L^2}\right]\right) \hat{\theta} \tag{5}$$

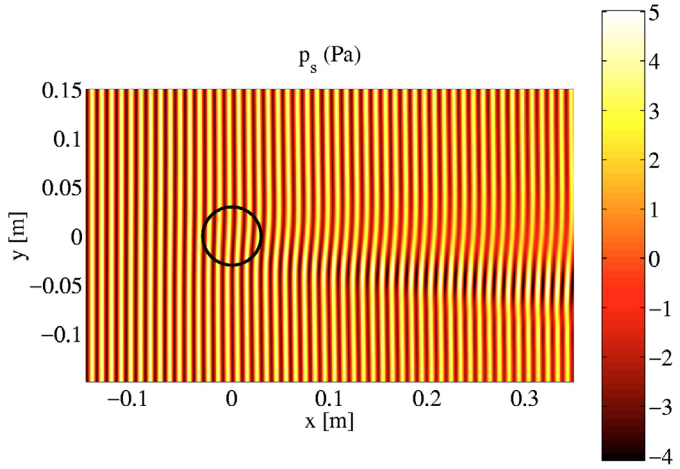

Fig. 2. Sound pressure p_s from the numerical experiment. The vortex is located at the circle position.

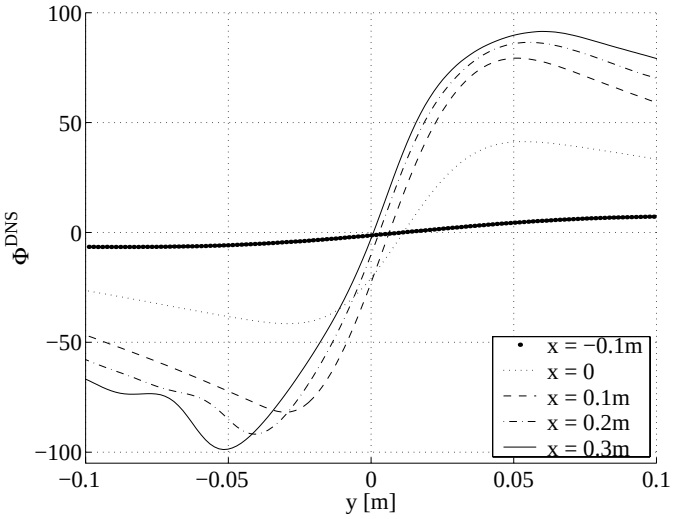

Fig. 3. Evolution of the phase shift Φ with the distance x from the vortex from the numerical data.

where $\hat{\theta}$ is the orthoradial unit vector and α is a constant roughly equal to 1.2 such that the velocity maximum v_m is located at $r = L$. Its circulation Γ and Mach number $\mathcal{M}$ are given by

$$\Gamma = \frac{\Omega_0 \pi L^2}{\alpha} \quad \text{and} \quad \mathcal{M} = \frac{|\Omega_0|\, L}{(1+2\alpha)\, c} \tag{6}$$

with c the speed of sound. The Oseen vortex typical size is $L \simeq 0.03$ m and its Mach number $\mathcal{M} = v_m/c \simeq 2.2\times10^{-2}$, close to the experimental Mach number. Ω_0 is determined by the value of $\mathcal{M}$ from the second part of equation (6) and equation (5) then gives the initial computational velocity field. The vortex is located at $(x_0 = 0.15\ \text{m}, y_0 = 0.15\ \text{m})$ from the South-West corner of the domain.

We choose a computational domain of size 0.5 m × 0.2 m, with a Cartesian mesh of 640×384 points to preserve a good numerical resolution of scattering phenomena. All the boundaries are non-reflecting and the West one models a plane wave emitter with wavelength $\lambda \simeq L/3$ and velocity amplitude $v_{inc} = 10^{-2}\ \text{m s}^{-1}$ as described in [23]. This amplitude choice ensures the linear behavior of sound waves.

The numerical microphones are spaced on lines $x = const.$ (x is the distance from x_0) from $x = -0.10$ m to $x = 0.35$ m.

4 Amplitude and phase of the sound wave

From the numerical data [26], we obtain the sound pressure p_s and the undisturbed plane incident sound pressure p_i. The sound pressure p_s is displayed in Figure 2. We observe that the vortical flow breaks the symmetry of the sound wave propagation with respect to the plane $y = 0$. The sound pressure amplitude becomes small in the vicinity of the forward direction whereas a maximum is observed along a constant angular direction. Moreover, the sound phase is twisted when the wave propagates through the vortex. The orientation of this twisting effect is related to the vortex flow, which rotates clockwise.

The sound pressure can be written, introducing the phase shift Φ between p_s and p_i and the normalized amplitude A_s with respect to the plane incident wave:

$$\frac{p_s}{p_i} = A_s\, \mathrm{e}^{\mathrm{i}\Phi} + \text{complex conjugate.} \tag{7}$$

Many temporal recordings of the sound waves are realized and we compute A_s^{DNS} and Φ^{DNS} from the DNS, using a numerical heterodyne detection. We can then extract the profiles $\Phi(y)$ of the phase shift as a function of the distance x from the vortex (Fig. 3). A phase jump is observed when the detector is displaced along the y-axis. This phase jump $\Delta\Phi$ increases as the sound wave travels away from the vortex position. We also observe that a significant part of the phase jump has been already generated when the wavefront reaches the center of the vortex $x = 0$. The largest part of the phase jump is produced by the interaction of the sound wave with the vortex core: the slow decay of the velocity field outside the core has just a small effect on the phase shift amplitude $\Delta\Phi$ (see also Fig. 2).

Following Klimov [27], we can consider the geometrical interaction of the incident wave (frequency ν_0, wavevector $\mathbf{k}_{inc}$) propagating through a mean flow $\mathbf{v}(\mathbf{r})$. In this limit, the mean flow acts on the sound wave in its direction of propagation like an optical refractive medium of variable index. Writing the incident wave in the form

$$\rho^k_{inc} = \rho_{inc_0}\, \exp\left[-\mathrm{i}(2\pi\nu_0)\, t + \mathrm{i}\mathbf{k}_{inc}\cdot\mathbf{r} + \mathrm{i}\phi^k(\mathbf{r})\right], \tag{8}$$

we can describe its phase evolution in the small Mach number limit by

$$\mathbf{k}_{inc}\cdot\boldsymbol{\nabla}\phi^k(\mathbf{r}) = -\frac{2\pi\nu_0}{c^2}\left[\mathbf{k}_{inc}\cdot\mathbf{v}(\mathbf{r})\right]. \tag{9}$$

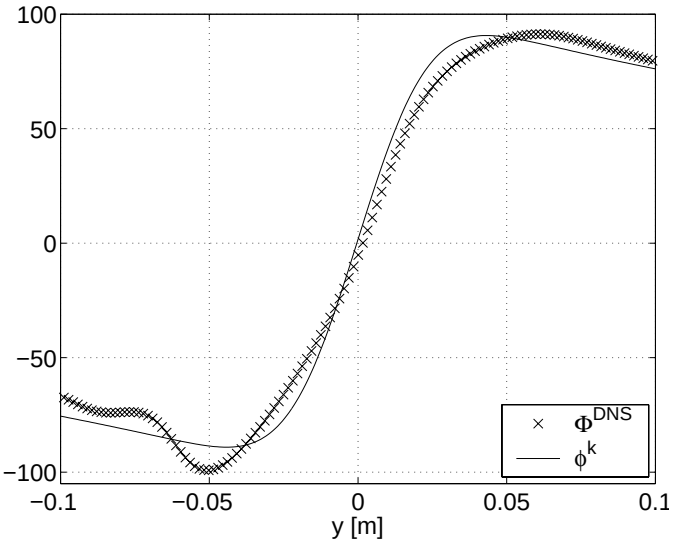

Fig. 4. Phase shift Φ from the numerical data and ϕ^k from equation (9), compared at $x/L = 10$ from the vortex.

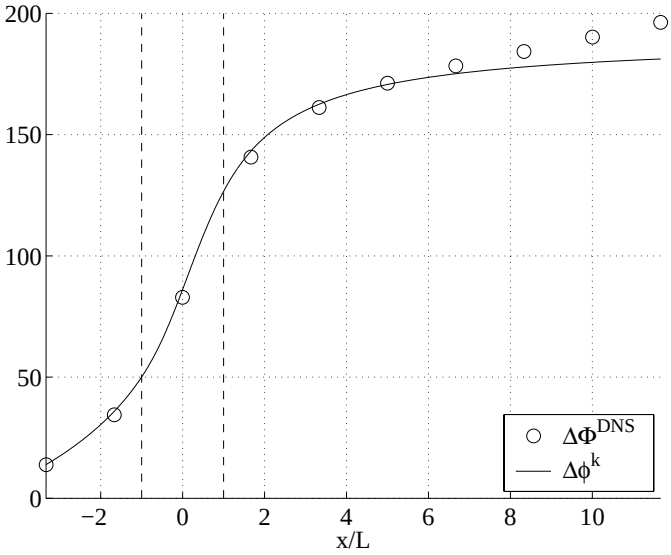

Fig. 5. Comparison of the phase jump of the sound wave deduced from the DNS (circles) with the phase jump of the incident wave deduced from the geometrical approach (9) (solid line). The vortex core is roughly located between the two dashed lines.

In the small Mach number limit, we can neglect the small tilt of $\mathbf{k}_{inc}$ from the $\hat{x}$ direction [28] and the incident phase at point $\mathbf{r} = (x, y)$ can be expressed as [29]

$$\phi^k(x,y) = -\frac{2\pi\nu_0}{c^2}\int_{-\infty}^{x} \mathbf{v}(x_1,y_1)\cdot\hat{x}\,\mathrm{d}x_1. \qquad (10)$$

We can then compute the phase $\phi^k(x, y)$ in the whole domain. We define the phase jump between the maximum and the minimum values of the phase (see Fig. 4) and we analyse the evolution of the phase jump $\Delta\phi^k$ with the distance from the vortex (Fig. 5). The quantitative agreement with the numerical result for Φ is good, except outside the vortex core. The geometrical phase jump $\Delta\phi^k$ corresponds to the dislocated wave produced by the vortex [30,31] whereas $\Delta\Phi^{DNS}$ also takes into account the wave scattered by the vortex core (see also Fig. 4). The scattering effects become important outside the first Fresnel zone [32]. This means $x/L \gg L/\lambda$ and corresponds to $x/L \gg 3$ in our computations.

Inserting the Oseen velocity field (5) in equation (10), we can calculate the phase $\phi^k(x, y)$:

$$\phi^k(x,y) = \frac{\Gamma\nu_0}{c^2}[\mathrm{Arctan}(x/y) + \mathrm{sign}(x/y)\,\pi/2 - y\,g(x,|y|)] \qquad (11)$$

where g is a function of x and $|y|$ which only depends on the internal structure of the vortex. Then, around the forward direction and far from the vortex location, the phase jump $\Delta\phi^k$ is

$$\Delta\phi^k = \frac{2\pi\nu_0\Gamma}{c^2}. \qquad (12)$$

Figure 5 shows that the phase jump $\Delta\Phi$ is mostly produced by the geometrical interaction of the sound wave

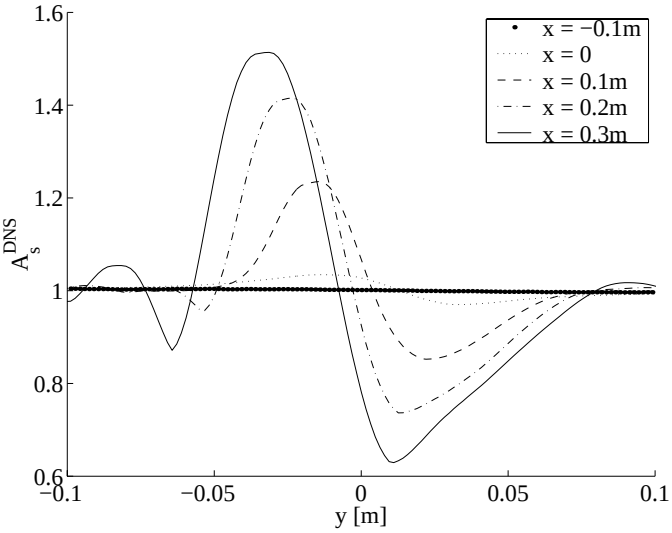

Fig. 6. Evolution of the amplitude ratio A_s with the distance x from the vortex from the numerical data.

even at a distance of observation ten times larger than the vortex radius.

We also extract the profiles $A_s(y)$ of the amplitude ratio as a function of the distance x from the vortex (Fig. 6). The evolution is rather different: as we go far from the vortex, both the amplitude maximum and minimum increase but the space lag between the two extrema remains almost constant. As can be seen in Figure 2, these effects are a consequence of the sound angular focusing by the vortex: as the velocity field induced by the vortex decays slowly, it has a long range interaction with the sound wave. Moreover, the amplitude changes become significant when the

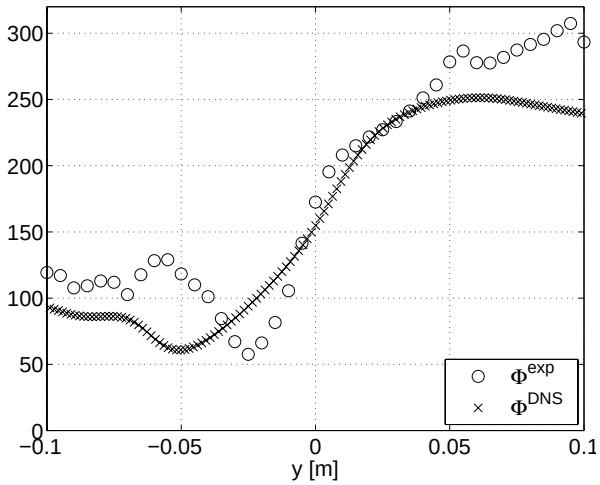

Fig. 7. Phase shifts Φ from numerical and experimental data.

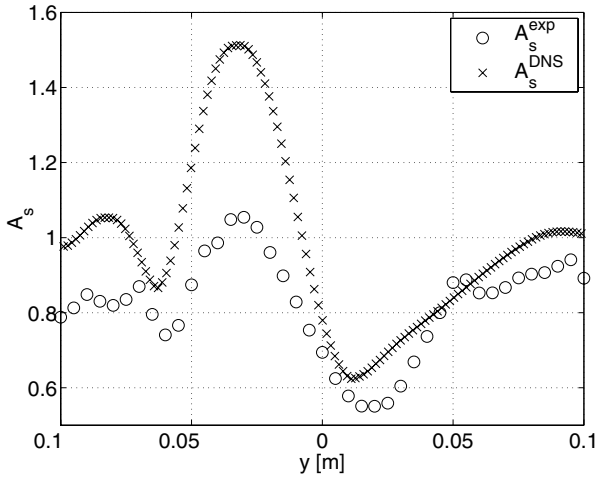

Fig. 8. Amplitude ratio A_s from numerical and experimental data.

sound has propagated through the entire vortex core. This is an important difference with the phase shift evolution: the scattered wave by the vortex is the only contribution to the amplitude evolution, whereas the phase jump, which is a purely kinematic effect, is also generated by the deformation of the incident wave.

5 Comparison with the experimental results

From the experimental data, we also obtain the sound pressure p_s and the undisturbed plane incident sound pressure p_i [33]. Then, from equation (7), we compute A_s^{exp} and Φ^{exp} using a numerical heterodyne detection and we can directly compare experimental and numerical results for the amplitude A_s and the phase shift Φ. This comparison is made up to a constant phase shift, due to the arbitrariness of the experimental phase reference. Also, a small lateral shift in the y coordinate is in order, to account for a misalignment in the zero reference for the detector position. To be close to the experimental situation, we realize the comparison for $x = 0.30$ m ($x/L = 30$).

DNS have been performed with various choice of λ/L and $\mathcal{M}$. The fit on the sound amplitude is very sensitive to the Mach number value and we choose $\mathcal{M} \simeq 2.2 \times 10^{-2}$, close to the experimental value. The value of L for the experimental setup cannot be accurately known, because the strong turbulent fluctuations in the velocity field preclude its accurate determination. We choose $\lambda/L \simeq 1/3$, which gives the best fit to the experimental data. Figure 7 shows the phase shift Φ from the numerical and the experimental results. The quantitative agreement is not excellent but the differences between Φ^{exp} and Φ^{DNS} are mostly outside the forward direction. They come from the small turbulent structures around the vortex that are not taken into account in the DNS. However, the phase jump $\Delta\Phi$ has the same order of magnitude in the experiment and in the DNS, showing that the dominant contribution is due to the mean flow. Thus, we can use its value, $\Delta\Phi^{exp} \simeq 200°$, to determine from equation (12) the order of magnitude of the mean flow circulation, $\Gamma \simeq 1.33\ \mathrm{m^2\,s^{-1}}$, in good agreement with hot wire measurements [19]. The maximum value of the velocity field cannot be easily deduced from Γ in the experimental case because the flow is turbulent around the vortex. We must take into account viscous effects and the mean vortex shape in the experiments is not exactly fitted by (4). However, using the above values of L and Γ gives a correct order of magnitude of the large scale velocity measured in the experiments [19].

The normalized amplitudes A_s^{exp} and A_s^{DNS} are plotted in Figure 8 under the same conditions of comparison. We observe larger difference between the experiment and the DNS on the sound amplitude than on its phase. The maximum amplitude value as well as the variations of the amplitude along the y-axis are much larger in the DNS. We think that this is due to the turbulent fluctuations which are not taken into account in the DNS. The Reynolds number of the experiment is larger than 10^5, thus the flow involves both a large scale vortex and turbulent fluctuations. These two components do not behave in the same way with respect to the scattering process. First, their typical time scales strongly differ: the turnover time in the vortex is roughly 1 ms, *i.e.* ten times larger than the travel time of the sound wave through it. The typical time scale of the smallest turbulent fluctuations is roughly 5×10^{-2} ms. Consequently, the turbulent flow configuration changes many times as the sound wave travels through the flow whereas the vortex looks frozen. Second, turbulent eddies involve a range of scales l_n smaller than the vortex radius L. Thus, $x \gg l_n^2/\lambda$ for a distance of observation $x/L = 10$ and there is a strong contribution of diffraction to the scattering by the small eddies [32]. We observe that scattering by random small scale eddies smooth out the amplitude variations along the y-axis whereas this does not affect the mean phase jump which primarily results from the coherent part of the flow, as it can be shown by taking the average of equation (10).

6 Conclusion

We have presented a study of sound propagation through a single vortex by direct numerical simulations (DNS). DNS allow the study of the sound-mean flow interaction within and near the vortex core, which is not feasible by direct measurements of the pressure field without strongly perturbating the flow. The vortical flow induces a phase jump in the sound wave and a strong angular focusing of the sound amplitude. The comparison with experimental measurements shows that the turbulent fluctuations tend to smooth the focusing of the sound amplitude. The phase jump, generated by the largest vortical structure, remains the same and turbulent fluctuations induce small variations on the phase shift. This allows the estimation of the vortex circulation by measuring the phase jump even when the surrounding flow is strongly turbulent.

This work has been partially supported by ECOS contract C98E04 and FONDECYT under grant number 1990169.

References

1. W. Baerg, W.H. Schwarz, J. Acoust. Soc. Am. **39**, 1125 (1966)
2. D.W. Schmidt, P.M. Tilmann, J. Acoust. Soc. Am. **47**, 1310 (1970)
3. M.S. Korman, R.T. Beyer, J. Acoust. Soc. Am. **67**, 1980 (1980)
4. B. Dernoncourt, J.-F. Pinton, S. Fauve, Physica D **117**, 181 (1998)
5. K. Oljaca, X. Gu, A. Glezer, M. Baffico, F. Lund, Phys. Fluids **10**, 4, 886 (1998)
6. C. Baudet, O. Michel, W.J. Williams, Physica D **128**, 1 (1999)
7. S. Manneville, J.H. Robres, A. Maurel, P. Petitjeans, M. Fink, Phys. Fluids **11**, 3380 (1999)
8. T.M. Georges, J. Acoust. Soc. Am. **51**, 206 (1972)
9. A.L. Fetter, Phys. Rev. A **136**, 1488 (1964)
10. G.M. Golemshtok, A.L. Fabrikant, Sov. Phys. Acoust. **26**, 209 (1980)
11. J. Reinschke, W. Möhring, F. Obermeier, J. Fluid. Mech **333**, 273 (1997)
12. R. Ford, S.G. Llewellyn Smith, J. Fluid. Mech. **386**, 305 (1999)
13. A.L. Fabrikant, Sov. Phys. Acoust. **29**, 152 (1983)
14. F. Lund, C. Rojas, Physica D **37**, 508 (1989)
15. P. Sakov, Sov. Phys. Acoust. **39**, 280 (1993)
16. R. Berthet, F. Lund, Phys. Fluids **7**, 2522 (1995)
17. D. Boyer, M. Baffico, F. Lund, Phys. Fluids **11**, 3819 (1999)
18. D. Boyer, F. Lund, Phys. Fluids **11**, 3829 (1999)
19. R. Labbé, J.F. Pinton, Phys. Rev. Let. **81**, 1413 (1998)
20. R. Labbé, J.F. Pinton, S. Fauve, Phys. Fluids **8**, 914 (1996)
21. S. Manneville, P. Roux, M. Tanter, A. Maurel, M. Fink, F. Bottausci, P. Petitjeans, Phys. Rev. E, **63**, 036607 (2001)
22. T. Colonius, S.K. Lele, P. Moin, J. Fluid. Mech **260**, 271 (1994)
23. Complete tests of the algorithm for sound scattering computations are presented in R. Berthet, D. Astruc, J.L. Estivalèzes, *Assessment of Numerical Boundary Conditions for Simulation of Sound Scattering by Vorticity*, 6th AIAA/CEAS Aeroacoustics Conference, AIAA-2000-2005 (2000) and in R. Berthet and D. Astruc, *Numerical boundary conditions for sound scattering simulation*, submitted to J. Comp. Phys. (2002)
24. L. Gamet, J.L. Estivalèzes, AIAA paper 95-0159 and references therein
25. G.K. Batchelor, *An Introduction to Fluid Dynamics*, Chap. 4.5 (Cambridge University Press, 1994)
26. The complete procedure to compute the sound quantities is described in [23] for the numerical simulation
27. V.V. Klimov, V.L. Prozorovskii, Sov. Phys. Acoust. **33**, 79 (1987)
28. In the geometrical limit, for $\mathcal{M} \ll 1$, the wavevector also gives the energy propagation direction and its tilt is proportional to the Mach number. See L. Landau, E. Lifchitz, *Cours de Physique Théorique*, Tome 6 *(Mécanique des Fluides)*, 2nd edn. (Éditions Mir, Moscou, 1989), Sect. 68
29. This equation can also be obtained in the geometrical limit of the sound-vortex interaction for $\mathcal{M} \ll 1$, with the acoustical ray formalism [21].
30. M.V. Berry, R.G. Chambers, M.D. Large, C. Upstill, J.C. Walmsley, Eur. J. Phys. **1**, 154 (1980)
31. R. Berthet, C. Coste, *Using a partial-wave method for sound-mean flow scattering problems*, Phys. Rev. E, in press (03-2003)
32. A. Ishimaru, *Wave Propagation and Scattering in Random Media*, Chap. 17 (Academic Press, 1978)
33. The complete procedure to compute the sound quantities is described in [19] for the experiment